Nonlinear Supersets to Droop Control

Mohit Sinha, Sairaj Dhople
Department of ECE
University of Minnesota
Email: sinha052, sdhople@umn.edu

Brian Johnson, Nathan Ainsworth
Power Systems Engineering Center
National Renewable Energy Laboratory
Email: brian.johnson, nathan.ainsworth@nrel.gov

Florian Dörfler
Automatic Control Laboratory
ETH Zürich
Email: dorfler@ethz.ch

***Abstract*—This paper offers a suite of extensions to Virtual Oscillator Control—a time-domain control method for islanded inverters whereby they are controlled to emulate the dynamics of weakly nonlinear limit-cycle oscillators. First, we develop a coordinate transformation to derive the PWM switching signals from the oscillator dynamic states in a manner that allows the inverter terminal-voltage amplitude and frequency to be traded off against a parametric linear combination of average active and reactive power. Additionally, we compare the time-domain performance of VOC to droop control for parallel connected inverters in two cases: synchronization from a cold start and inverter addition. Finally, with a view towards developing output-filter-design strategies as well as outlining strategies for grid-connected operations, we derive a sufficient condition for a Virtual-Oscillator-controlled inverter to be entrained to a stiff voltage source.**

I. Introduction

The goal of decentralized real-time control in islanded power-electronics based systems is to regulate the constituent inverters' terminal-voltage amplitude and frequency. Most literature in this domain focuses on incarnations of *droop control* [1]–[4]; wherein inverter active- and reactive-power injections are linearly traded off with terminal voltage and frequency. Markedly different from droop control—which relies on phasor quantities that are only well defined in quasi steady state—a compelling time-domain alternative is to control the inverters to emulate the dynamics of weakly nonlinear Liénard-type limit-cycle oscillators [5]. This method is termed *Virtual Oscillator Control* (VOC). It is implemented by programming the dynamics of the oscillators onto the inverters' microcontrollers, and utilizing sinusoidally varying oscillator states to construct pulse-width modulation (PWM) control signals. Our previous efforts have established several advantages of VOC including the ability to: i) stabilize arbitrary initial conditions to a stable sinusoidal steady state [6], ii) achieve system-wide synchrony without any communication [7], and iii) contend with linear and nonlinear loads [5]. In this paper, we offer some extensions to our previous work that facilitate design and simplify analysis of VOC.

Recently, we proved that droop laws in resistive networks (where real power is traded off for voltage amplitude and reactive power is traded off for frequency) can be uncovered in the averaged sinusoidal-steady-state dynamics of Van der Pol oscillators [6]. Building upon this, we develop an extension that allows one to recover a whole family of droop relations (e.g., real power can be traded off for frequency and reactive power for voltage, as would be desired in inductive networks). The approach is based on constructing the inverter PWM switching signals by formulating a coordinate transformation that implements an angular displacement of the oscillator dynamic states. As the angular displacement is varied, we show that the VOC dynamics in sinusoidal steady state vary from mimicking droop laws in resistive networks to those in inductive networks. In essence, we demonstrate that the coordinate transformation allows one to recover a suite of nonlinear supersets to droop control. Using the resultant model, we present a running example for designing VOC for inductive networks which complements our recent work in [8] where we presented design strategies for resistive networks.

As a second contribution, we provide time-domain simulations to compare VOC with droop control for a parallel system of inverters serving a resistive load. We investigate two cases: i) synchronization from a cold start and arbitrary initial conditions, and ii) addition of an inverter to an already synchronized system. We show that VOC outperforms droop control in both the cases since the phase-synchronized equilibrium is attained much faster. It should be noted that the comparison is performed for inverters where sinusoidal steady-state regulation characteristics of both VOC and droop control are engineered to be approximately equivalent.

Finally, to further formalize design approaches for VOC, we derive a sufficient condition that establishes when a VO-controlled inverter with an LCL output filter will be entrained with a stiff voltage source with a given frequency and voltage. Our analysis leverages classical results on entrainment of Van der Pol oscillators [9]. Simulation results indicate the lower bound on the amplitude of the driving voltage source to guarantee synchronization for a small frequency difference. This analysis not only yields insights into the design of output filters, but it also paves the way to explore multi-mode (grid-connected and islanded) operation.

The remainder of the paper is organized as follows. Section II introduces VOC and delineates the dynamical model that captures the inverters AC-time scale behaviour. Using the model, tunable voltage- and frequency regulation characteristics are derived and are subsequently leveraged to formulate a VOC design strategy for inductive networks. In Section III, simulation results in the time domain are provided to compare the performance of VOC and droop control. Section IV presents results on entrainment. Finally, we conclude the paper by outlining a few directions for future work in Section V.

978-1-4673-6847-6/15/$31.00 ©2015 IEEE

II. Tunable Droop Relations

In this section, we outline the dynamical model that captures the AC time-scale behavior of the inverter terminal voltage. We parametrize the model by introducing a 2-D rotation matrix for coordinate transformation. The ensuing coordinate-transformed model establishes a relationship between the inverter terminal-voltage amplitude and frequency with the average real- and reactive-power output as a function of the rotation angle. This enables one to obtain tunable voltage- and frequency-regulation characteristics, and potentially synthesize a family of nonlinear supersets to droop control. We begin with a brief overview of VOC.

A. Controller Implementation

Figure 1 illustrates the implementation of VOC for a single-phase inverter. The closed-loop controller is a discretized version of the Van der Pol oscillator dynamics programmed on the digital microcontroller. The virtual oscillator circuit is composed of a parallel connection of: i) a harmonic oscillator with inductance, L, and capacitance, C (with unforced frequency $\omega = 1/\sqrt{LC}$); ii) a negative conductance $-\sigma$; and iii) a cubic voltage dependent current source, $\alpha v_{\rm C}^3$, where $v_{\rm C}$ is the capacitor voltage and α is a positive real constant. The virtual oscillator is coupled to the physical signals in the inverter through the current and voltage scalings, $\kappa_{\rm i}$ and $\kappa_{\rm v}$ respectively, as well as a rotation matrix Ξ about an angle φ. The virtual capacitor-voltage, $v_{\rm C}$, and inductor-current, $i_{\rm L}$, are used to construct the signal v (we elaborate on this in the next section) which is used to generate the PWM signal.

B. Dynamical Model

We begin by writing the circuit equations that describe the operation of the virtual oscillator circuit. The dynamics of the virtual-oscillator inductor current, i_L, and virtual-oscillator capacitor voltage, v_C, are:

$$L\frac{di_L}{dt} = v_C, \quad C\frac{dv_C}{dt} = -\alpha\frac{v_C^3}{\kappa_{\rm v}^3} + \sigma v_C - i_L - \kappa_{\rm i} i\,. \tag{1}$$

We introduce the following definitions to simplify notation:

$$\varepsilon := \sqrt{\frac{L}{C}}, \quad g(y) := y - \frac{\beta}{3}y^3, \quad \beta := \frac{3\alpha}{\kappa_{\rm v}^2\sigma}. \tag{2}$$

A state-space model of the VO-controlled inverter in Cartesian coordinates can be formulated with scaled versions of the virtual inductor current and the virtual capacitor voltage selected as states, $x := \kappa_{\rm v}\varepsilon i_L$, and $y := \kappa_{\rm v} v_C$. With the aid of $g(\cdot)$ and ε defined in (2), (1) can be rewritten in the time coordinates $\tau = \omega t = (1/\sqrt{LC})t$ as follows:

$$\dot{x} = \frac{dx}{d\tau} = y, \quad \dot{y} = \frac{dy}{d\tau} = -x + \varepsilon\sigma g(y) - \varepsilon\kappa_{\rm v}\kappa_{\rm i} i. \tag{3}$$

The system dynamics can now be represented on the polar plane as shown in Fig. 1(b) where $\sqrt{2}V = (x^2+y^2)^{1/2}$. The x and y coordinates are orthogonal and can be expressed as

$$\begin{aligned} x(t) &= \sqrt{2}V(t)\sin(\omega t + \theta(t)) = \sqrt{2}V(t)\sin(\phi(t)),\\ y(t) &= \sqrt{2}V(t)\cos(\omega t + \theta(t)) = \sqrt{2}V(t)\cos(\phi(t)), \end{aligned} \tag{4}$$

where ω is the electrical frequency, $\theta(t)$ represents the phase offset with respect to ω, and $\phi(t)$ is the instantaneous phase angle.

As shown in Fig. 1, we utilize a 2-D rotation to define another set of orthogonal signals, $v(t)$ and $v^{\perp}(t)$, where $v(t)$ will subsequently be used to control the inverter terminal voltage. The values of v and $v^{\perp}$ can be written in terms of the states x and y using the *rotation matrix*, Ξ, as:

$$\begin{bmatrix} v \\ v^{\perp} \end{bmatrix} = \begin{bmatrix} \cos\varphi & \sin\varphi \\ -\sin\varphi & \cos\varphi \end{bmatrix} \begin{bmatrix} y \\ x \end{bmatrix} =: \Xi \begin{bmatrix} y \\ x \end{bmatrix}. \tag{5}$$

To extract amplitude and phase information, we transform the voltage signal, v, and its corresponding orthogonal signal, $v^{\perp}$, to polar coordinates as: $v = \sqrt{2}V\cos(\phi+\varphi)$, and $v^{\perp} = \sqrt{2}V\sin(\phi+\varphi)$. Differentiating the identities: $\sqrt{2}V = \sqrt{x^2+y^2}$ and $\phi = \tan^{-1}\frac{x}{y}$, we obtain the dynamical equations for V and ϕ as:

$$\begin{aligned} \dot{V} &= \frac{\varepsilon}{\sqrt{2}}\Big(\sigma g\big(\sqrt{2}V\cos(\phi)\big) - \kappa_{\rm v}\kappa_{\rm i} i\Big)\cos(\phi), \\ \dot{\phi} &= 1 - \frac{\varepsilon}{\sqrt{2}V}\Big(\sigma g\big(\sqrt{2}V\cos(\phi)\big) - \kappa_{\rm v}\kappa_{\rm i} i\Big)\sin(\phi). \end{aligned} \tag{6}$$

We operate in the $\varepsilon \searrow 0$ regime to ensure dynamics that mimic those of a harmonic oscillator [10]. Furthermore, we average the dynamics in (6) to focus on AC-cycle time scales. The resulting autonomous system is much easier to analyze than the time-varying system (without compromising much on the accuracy as the analysis is correct up to $\mathcal{O}(\varepsilon)$) [11]. Let us denote $\overline{V}$ and $\overline{\theta}$ to be 2π-averaged values of V and θ. Then, recognizing that $\varepsilon \searrow 0$, we can write the averaged dynamics as [11, Theorem 10.4] [6], [12]:

$$\begin{bmatrix} \dot{\overline{V}} \\ \dot{\overline{\theta}} \end{bmatrix} = \frac{\varepsilon\sigma}{2}\begin{bmatrix} \overline{V} - \frac{\beta}{2}\overline{V}^3 \\ 0 \end{bmatrix} - \frac{\varepsilon\kappa_{\rm v}\kappa_{\rm i}}{2\pi\sqrt{2}}\int_0^{2\pi} i \begin{bmatrix} \cos(\tau+\overline{\theta}) \\ -\frac{1}{\overline{V}}\sin(\tau+\overline{\theta}) \end{bmatrix} d\tau. \tag{7}$$

Since we are interested in uncovering the relationship between terminal voltage and power, we define the instantaneous active- and reactive-power injections [13], [14] as:

$$P(t) = v(t)i(t), \quad Q(t) = v(t-\pi/2)i(t) =: v^{\perp}(t)i(t), \tag{8}$$

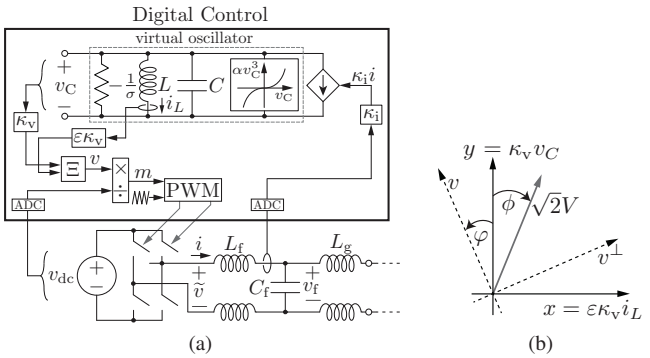

Figure 1: (a) Implementation of VOC on a single-phase H-bridge inverter with LCL output filter. (b) The matrix, Ξ, *rotates* the capacitor voltage and inductor current to yield the commanded inverter terminal voltage $v(t)$.

where $i(t)$ is the output current. The average real and reactive power over an AC cycle of period $2\pi/\omega$ are:

$$\overline{P} = \frac{\omega}{2\pi}\int_{s=0}^{2\pi/\omega} P(s)ds, \quad \overline{Q} = \frac{\omega}{2\pi}\int_{s=0}^{2\pi/\omega} Q(s)ds. \tag{9}$$

Transitioning (7) from τ to t coordinates, retaining only $\mathcal{O}(\varepsilon)$ terms, and using the definitions of active and reactive power in (8), we get:

$$\begin{aligned}\frac{d}{dt}\overline{V} &= \frac{\sigma}{2C}\left(\overline{V} - \frac{\beta}{2}\overline{V}^3\right) - \frac{\kappa_{\rm v}\kappa_{\rm i}}{2C}\left(\cos\phi\frac{\overline{P}}{\overline{V}} + \sin\phi\frac{\overline{Q}}{\overline{V}}\right),\\ \frac{d}{dt}\overline{\theta} &= \frac{\kappa_{\rm v}\kappa_{\rm i}}{2C}\left(-\sin\phi\frac{\overline{P}}{\overline{V}^2} + \cos\phi\frac{\overline{Q}}{\overline{V}^2}\right).\end{aligned} \tag{10}$$

Thus, we obtain terminal-voltage amplitude and frequency dynamics that are linked to active- and reactive-power outputs at the inverter terminals through the 2-D rotation matrix, Ξ. The steady-state voltage- and frequency-regulation equations are equilibrium points of the system in (10):

$$\begin{aligned}\sigma\overline{V}_{\rm eq} - \frac{\sigma\beta}{2}\overline{V}_{\rm eq}^3 - \kappa_{\rm v}\kappa_{\rm i}\begin{bmatrix}\cos\varphi\\ \sin\varphi\end{bmatrix}^{\rm T}\begin{bmatrix}\frac{\overline{P}_{\rm eq}}{\overline{V}_{\rm eq}}\\ \frac{\overline{Q}_{\rm eq}}{\overline{V}_{\rm eq}}\end{bmatrix} &= 0\ ,\\ \omega_{\rm eq} - \omega - \frac{\kappa_{\rm v}\kappa_{\rm i}}{2C}\begin{bmatrix}-\sin\varphi\\ \cos\varphi\end{bmatrix}^{\rm T}\begin{bmatrix}\frac{\overline{P}_{\rm eq}}{\overline{V}^2_{\rm eq}}\\ \frac{\overline{Q}_{\rm eq}}{\overline{V}^2_{\rm eq}}\end{bmatrix} &= 0,\end{aligned} \tag{11}$$

with $\overline{V}_{\rm eq}$, $\overline{P}_{\rm eq}$, and $\overline{Q}_{\rm eq}$ denoting RMS voltage amplitude, average real- and reactive-power output respectively, and $\omega_{\rm eq}$ is the steady-state frequency. With appropriate decoupling assumptions, various droop-like laws can be recovered from (11): with $\varphi = \pi/2$ we get that terminal voltage is traded off for reactive power and frequency is traded off for active power; similarly, with $\varphi = 0$, we see that terminal voltage is traded off for active power and frequency is traded off for reactive power. These are reminiscent of the ubiquitous droop control laws for inductive (respectively, resistive) line impedances.

C. VOC Design for Inductive Networks

The averaged models reveal conclusive links between real- and reactive-power outputs and the terminal-voltage dynamics; and therefore, they suggest avenues to design the virtual oscillators so that the controlled inverter satisfies performance requirements. With reference to the model in (11), for the case where $\varphi = 0$, we formulated a design strategy for inverters to satisfy performance specifications related to voltage regulation, frequency regulation, dynamic response, and harmonic content in [8]. Here, we explore an analogous design strategy for the case $\varphi = \pi/2$; which is applicable to inductive networks.

Accompanying the design strategy to pick system parameters, we present a running example for VOC design corresponding to the following set of performance specifications: rated real power $750\,\mathrm{W}$, rated reactive power $750\,\mathrm{VAR}$, voltage-regulation of $\pm 5\%$ around a nominal voltage of $120\,\mathrm{V}$, frequency-regulation of $\pm 0.5\,\mathrm{Hz}$ around a nominal frequency of $60\,\mathrm{Hz}$, rise-time of $0.1\,\mathrm{s}$, ratio of third-to-first harmonic 2% and load sharing in a parallel setting. The design is subsequently validated by a switching-level simulation in MATLAB.

With the choice $\varphi = \pi/2$, the expressions in (11) boil down to the following:

$$\sigma\overline{V}_{\rm eq} - \frac{\sigma\beta}{2}\overline{V}_{\rm eq}^3 - \kappa_{\rm v}\kappa_{\rm i}\frac{\overline{Q}}{\overline{V}_{\rm eq}} = 0, \tag{12}$$

$$\omega_{\rm eq} - \omega + \frac{\kappa_{\rm v}\kappa_{\rm i}}{2C}\frac{\overline{P}}{\overline{V}^2_{\rm eq}} = 0\,. \tag{13}$$

To standardize design, we choose $\kappa_{\rm v}$, so that when the VO capacitor voltage is $1\,\mathrm{V}$ RMS, the output voltage is the open-circuit voltage, $\overline{V}_{\rm oc}$. Furthermore, we pick $\kappa_{\rm i}$ so that the output current is $1\,\mathrm{A}$, when rated reactive power, $\overline{Q}_{\rm rated}$, is drawn from it. Thus, the choice of $\kappa_{\rm v}$ and $\kappa_{\rm i}$ are taken to be:

$$\kappa_{\rm v} = \overline{V}_{\rm oc},\ \kappa_{\rm i} = \frac{\overline{V}_{\rm min}}{|\overline{Q}_{\rm rated}|}. \tag{14}$$

For this choice, let us calculate σ in terms of $\overline{V}_{\rm min}$, which is the inverter terminal voltage when rated reactive power is drawn from it. Rearranging the terms and substituting values of $\kappa_{\rm v}$ and $\kappa_{\rm i}$ in voltage regulation equation gives

$$\sigma = \frac{\overline{V}_{\rm oc}^3}{\overline{V}_{\rm min}(\overline{V}_{\rm oc}^2 - \overline{V}_{\rm min}^2)}\,. \tag{15}$$

Upon substituting $\overline{V}_{\rm oc} = 120\,\mathrm{V}$ and $\overline{V}_{\rm min} = 114\,\mathrm{V}$, we get $\sigma = 10.79$.

To quantify the dynamic response of the VO-controlled inverter, we analyse how quickly the terminal voltage rises to the open-circuit voltage. We define *rise time*, denoted by $t_{\rm rise}$, as the time taken for the inverter terminal voltage to rise from $0.1\overline{V}_{\rm oc}$ to $0.9\overline{V}_{\rm oc}$. Furthermore, we capture and quantify the harmonic content of the terminal voltage through the ratio of the amplitude of the third-harmonic to the fundamental, $\delta_{3:1}$. Following the analysis in [8] for rise-time and harmonic content in the terminal voltage for an unloaded inverter, we have:

$$t_{\rm rise} \approx \frac{6C}{\sigma},\ \delta_{3:1} \approx \frac{\sigma}{8\omega C}, \tag{16}$$

where ω is the nominal frequency. Thus, upon imposing the design requirements (rise-time of $0.1\,\mathrm{s}$, ratio of third-to-first harmonic 2%), we get from (16):

$$\frac{10}{192\pi} \le \frac{C}{\sigma} \le \frac{1}{60}\,. \tag{17}$$

Also, to ensure frequency-regulation of $\pm 0.5\,\mathrm{Hz}$, the following must hold:

$$C \ge \frac{1}{4\pi 0.5}\frac{\overline{V}_{\rm oc}}{\overline{V}_{\rm min}}\frac{\overline{P}_{\rm rated}}{|\overline{Q}_{\rm rated}|}, \tag{18}$$

where we have substituted for $\kappa_{\rm v}$ and $\kappa_{\rm i}$ from (14) in (13) and assumed the worst-case operating condition that maximum average active power, $\overline{P}_{\rm rated}$, is sourced at the minimum permissible terminal voltage $\overline{V}_{\rm min}$. We, therefore, fix $C = 10.79/60\,\mathrm{F}$ which the satisfies lower bound specified by (18).

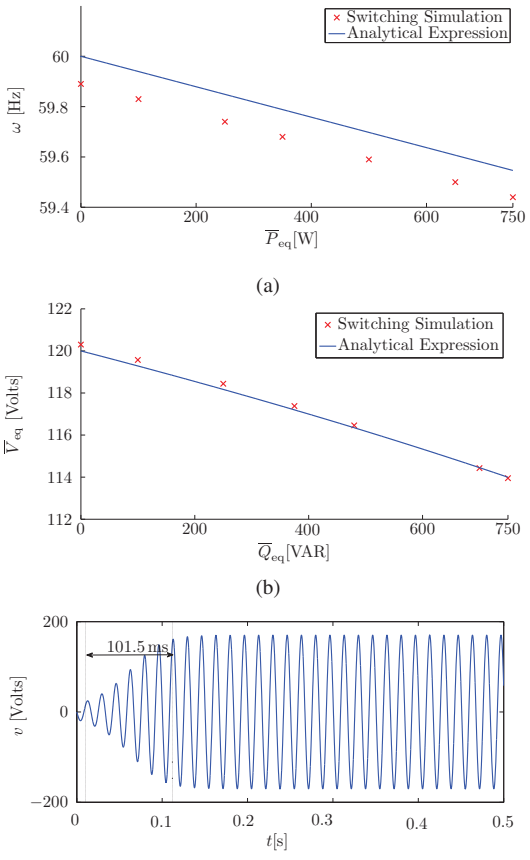

Figure 2: Switching-level simulations to validate the inductive droop characteristic derived analytically: (a) Frequency regulation, (b) Voltage regulation, and (c) Rise time.

Simulation Results: To validate the design strategy, we perform a switching-time-scale simulation in MATLAB. The filter components are chosen as $L_{\rm f} = 1.8\,{\rm mH}$, $C_{\rm f} = 25\,\mu{\rm F}$, and $L_{\rm g} = 0.9\,{\rm mH}$ where $L_{\rm f}$, $C_{\rm f}$, and $L_{\rm g}$ are the inverter-side inductor, ac-filter capacitor, and grid-side inductor, respectively (see Fig. 1 (a)). Figures 2 (a) and (b) depict the frequency- and voltage-regulation equations for the VO-controlled inverter. In Fig. 2 (a), the slope of the curve closely matches with the analytical expression. However, there is a constant error of $0.1\,{\rm Hz}$ which we attribute to the PLL (that is used to compute the frequency) and numerical solvers used in the simulation. Figure 2 (b) shows the obtained voltage-regulation curve. Lastly, the time-domain voltage waveform in Fig. 2 (c) shows a rise-time of $0.102\,{\rm s}$ (closely matching the desired value of $0.1\,{\rm s}$).

III. Time Domain Comparison with Droop Control

In this section, we present simulation results with switching-level fidelity to compare droop control and VOC in the time domain. Our simulation study is focused on comparing the time to synchronize parallel-connected single-phase inverters serving a resistive load (from a cold start and also for inverter addition) with the two control strategies.

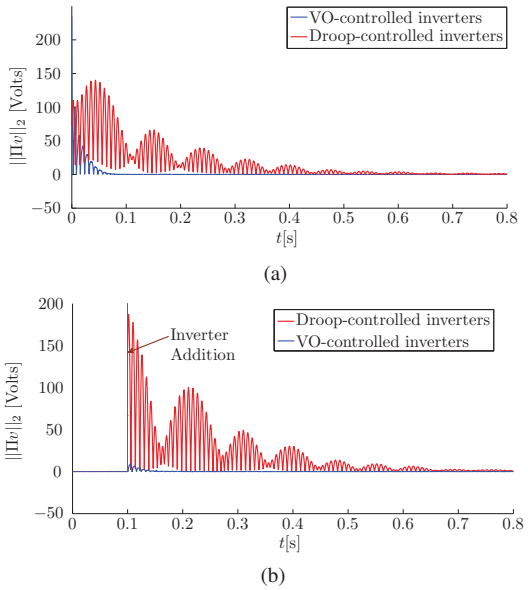

Figure 3: Switching-level simulations illustrate the synchronization error for VO-controlled inverters and droop-controlled inverters for: (a) startup from random initial conditions, and (b) inverter addition.

A. Controller Description

We begin with a description of the droop controller and VOC controller. Note that the VOC controller is designed so that it offers approximately the same voltage and frequency regulation as the droop controlled inverter. (See [8] for details.)

Droop control: For the droop controller implementation, we choose the so-called *universal droop laws* [15] given by:

$$\begin{aligned} \overline{V}_{\rm eq} &= \overline{V}^* + m_{\rm P}\overline{P}_{\rm eq}\,, \\ \omega_{\rm eq} &= \omega^* + m_{\rm Q}\overline{Q}_{\rm eq}\,. \end{aligned} \tag{19}$$

The real- and reactive-power inputs to the droop controller are determined by integrating the product of output current injection and the inverter terminal voltage and its quadrature component over an AC cycle, respectively (see equations (8)-(9)). The quadrature component of the voltage is derived by using a second-order generalized integrator. Additionally, the real- and reactive-power calculations are filtered through a low pass filter with cut-off frequency, $\omega_{\rm c}$ [16].

Virtual Oscillator Control: Next, we design a virtual oscillator controller that emulates the steady-state characteristics of the droop controller by using the analysis outlined in Appendix C of [8]. The choice of σ and C are based on the choice of droop coefficients and is derived using the relation:

$$\sigma = -m_{\rm P}^{-1}\frac{\kappa_{\rm i}}{2},\ C = m_{\rm Q}^{-1}\frac{\kappa_{\rm i}}{2\overline{V}_{\rm oc}}. \tag{20}$$

Given which, L can be determined for the nominal system frequency, ω.

The parameters adopted for the simulations that are outlined next are as follows: $\varphi = 0$, $\overline{V}_{\rm oc} = 126\,{\rm V}$, $\omega = 2\pi\,60\,{\rm rad/s}$, $m_{\rm P} = -0.008$, $m_{\rm Q} = 0.01$, $\kappa_{\rm v} = 126\,{\rm V/V}$, $\kappa_{\rm i} = 0.152\,{\rm A/A}$, $\sigma = 9.5\,\Omega^{-1}$, $\alpha = 6.333\,{\rm A/V^3}$, $C = 0.0603\,{\rm F}$, $L =$

$0.117\,\mathrm{mH}$, $R_{\mathrm{load}} = 220\,\Omega$, Switching frequency $f_{\mathrm{sw}} = 15\,\mathrm{kHz}$, $L_{\mathrm{f}} = 1.8\,\mathrm{mH}$, $L_{\mathrm{g}} = 0.9\,\mathrm{mH}$, $C_{\mathrm{f}} = 25\,\mu\mathrm{F}$, low pass filter for real- and reactive-power calculations for droop controller, $H_{\mathrm{f}}(s) = \omega_{\mathrm{c}}/(s+\omega_{\mathrm{c}})$ with $\omega_{\mathrm{c}} = 2\pi\,10\,\mathrm{rad/s}$.

To compare the strategies, we illustrate synchronization error with the aid of the quantity $||\Pi v||_2$, where v is the N-dimensional vector that collects the inverter terminal voltages. The matrix $\Pi := I_{\mathrm{N}} - \frac{1}{N} 1_{\mathrm{N}} 1_{\mathrm{N}}^{\mathrm{T}}$ (I_N is the $N \times N$ identity, and $1_{N\times 1}$ is the $N \times 1$ vector with all entries equal to one) is the so-called projector matrix, and by construction, we see that Πv returns a vector where the entries capture deviations from the average of the entries in the vector v.

B. Synchronization from a Cold Start

In Fig. 3 (a) we plot the synchronization error for a collection of $N = 3$ inverters from a cold start with arbitrary initial conditions. It is evident that the voltages synchronize faster with VOC. In particular, with VOC, the inverters synchronize by around $t = 0.05\,\mathrm{s}$, while with droop control, the inverters synchronize by $t = 0.6\,\mathrm{s}$. We point out that the error magnitude, i.e., $\|\Pi v\|_2$, at $t = 0$ for droop control is $71.7\,\mathrm{V}$, significantly lower than $234.8\,\mathrm{V}$ for VOC.

C. Inverter Addition

Now, we consider the case of adding a fourth inverter to the already synchronized system of three-inverters. At $t = 0$, both the systems (droop control and VOC) are perfectly synchronized with $\|\Pi v\|_2 \approx 0$. At $t = 0.1\,\mathrm{s}$, a fourth inverter (starting from an arbitrary initial condition) is added to the system and the deviation of the terminal voltages of the four inverters from the average are plotted against time for droop control and VOC. From Fig. 3(b), it can be clearly seen that VO-controlled inverters synchronize and reach the phase-synchronized equilibrium considerably faster than those controlled with droop control.

IV. Entrainment

In this section, we derive a sufficient condition for synchronizing the inverter to an external stiff voltage source. The stiff voltage source can be assumed to model a circuit equivalent of the microgrid electrical network. The results below can therefore also be interpreted as stability of the nonlinear control strategy.

A. Entrainment of Van der Pol Oscillators

To develop the analysis, we leverage classical results on the entrainment property of Van der Pol oscillators, which refers to the case when the oscillator becomes frequency-locked to the external forcing function. In a nutshell, the result indicates that if the forcing is strong enough, and the frequency difference between the unforced limit cycle oscillation and the forcing function is small enough, then one can recover oscillations at the forcing frequency. A precise statement follows next.

Lemma 1. *Consider a forced Van der Pol oscillator, with dynamics described by the following differential equation:*

$$\frac{d^2x}{dt^2} + x - \epsilon\sigma(1-\beta x^2)\frac{dx}{dt} = \epsilon F\cos\omega t\,, \tag{21}$$

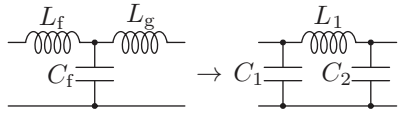

Figure 4: Illustrating the output-filter transformation.

where $\epsilon > 0$ is sufficiently small. Assume that the forcing frequency, ω, is nearly equal to the the unforced limit cycle frequency (given by the unit frequency) up to order $\mathcal{O}(\epsilon^2)$, that is, $\omega = 1 + k\epsilon + \mathcal{O}(\epsilon^2)$ for some $k \in \mathbb{R}$. Then, if

$$F^2 > \sigma^2\left(\frac{\sqrt{\beta}}{2} + \frac{2}{\sqrt{\beta}} - 2\right) + \frac{8k^2}{\sqrt{\beta}}\,, \tag{22}$$

the Van der Pol oscillator (21) *exhibits oscillations at the frequency ω of the external forcing function.*

Proof. See [9], [17] for a proof. □

B. Entrainment of VO-Controlled Inverters

Assume $\varphi = 0$ (without any loss of generality) and suppose that the output of the inverter is connected to a voltage source $v_{\mathrm{g}} := V_{\mathrm{g}}\cos(\omega_{\mathrm{g}} t)$ through an LCL filter with reactances, L_{f}, L_{g}, and C_{f}, as shown in Fig 1 (a). To facilitate analysis, we transform the LCL filter with a $\mathcal{T}$ topology, to an approximate CLC filter with Π topology as shown in Fig. 4.[1] The filter elements corresponding to the CLC filter are given by

$$C_1 = \frac{C_{\mathrm{f}}L_{\mathrm{g}}}{L_{\mathrm{g}}+L_{\mathrm{f}}},\ C_2 = \frac{C_{\mathrm{f}}L_{\mathrm{f}}}{L_{\mathrm{g}}+L_{\mathrm{f}}},\ L_1 = L_{\mathrm{f}} + L_{\mathrm{g}}. \tag{23}$$

Circuit equations corresponding to the equivalent filter arrangement can be written as:

$$\begin{aligned} L\frac{di_{\mathrm{L}}}{dt} &= \frac{v}{\kappa_{\mathrm{v}}}\,,\\ C\frac{dv}{dt} &= -\frac{\alpha v^3}{\kappa_{\mathrm{v}}^2} + \sigma v - \kappa_{\mathrm{v}} i_{\mathrm{L}} - \kappa_{\mathrm{v}}\kappa_{\mathrm{i}} i\,,\\ \frac{di}{dt} &= \frac{v - v_{\mathrm{g}}}{L_1} + C_1\frac{d^2v}{dt^2}\,, \end{aligned} \tag{24}$$

and, therefore, the system can be compactly described by

$$\frac{d^2v}{d\tau^2} - \varepsilon'\sigma\left(1-\beta v^2\right)\frac{dv}{d\tau} + v = \frac{\varepsilon'\kappa_{\mathrm{v}}\kappa_{\mathrm{i}}}{L_1\omega_{\mathrm{f}}}V_{\mathrm{g}}\cos\left(\frac{\omega_{\mathrm{g}}}{\omega_{\mathrm{f}}}\tau\right)\,, \tag{25}$$

where we have re-scaled the original equations with respect to time by defining $\tau := \omega_{\mathrm{f}} t$. The parameters ε' and ω_{f} are

$$\varepsilon' = \sqrt{\frac{L_{\mathrm{eq}}}{C_{\mathrm{eq}}}},\ \omega_{\mathrm{f}} = \frac{1}{\sqrt{L_{\mathrm{eq}}C_{\mathrm{eq}}}}, \tag{26}$$

with C_{eq} and L_{eq} given by:

$$C_{\mathrm{eq}} = C + \kappa_{\mathrm{v}}\kappa_{\mathrm{i}}C_1,\ L_{\mathrm{eq}} = \left(\frac{1}{L} + \frac{\kappa_{\mathrm{v}}\kappa_{\mathrm{i}}}{L_1}\right)^{-1}. \tag{27}$$

[1]To facilitate this transformation and the ensuing analysis, we need to assume $j\omega L_{\mathrm{f}} << \frac{1}{j\omega}\frac{L_{\mathrm{f}}}{C_{\mathrm{f}}L_{\mathrm{g}}} + \frac{1}{j\omega C_{\mathrm{f}}}$, $j\omega L_{\mathrm{g}} << \frac{1}{j\omega}\frac{L_{\mathrm{g}}}{C_{\mathrm{f}}L_{\mathrm{f}}} + \frac{1}{j\omega C_{\mathrm{f}}}$, and $j\omega\left(L_{\mathrm{f}} + L_{\mathrm{g}}\right) >> -j\omega^3 L_{\mathrm{f}}L_{\mathrm{g}}C_{\mathrm{f}}$. We remark that these inequalities are typically satisfied in practical implementations.

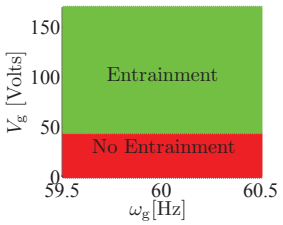

Figure 5: The space of feasible forcing amplitudes required to synchronize the inverter to the stiff voltage source is plotted for a range of grid frequencies ranging from $59.5\,\mathrm{Hz}$ to $60.5\,\mathrm{Hz}$.

Now, consider the following result which establishes a parametric sufficient condition for the voltage of the inverter to frequency synchronize with the stiff voltage source.

Corollary 1. *Consider the forced nonlinear dynamical system described by* (25)*. Assume the frequency of the stiff voltage source, ω_g, and the frequency of the VO-controlled inverter, ω_f, are sufficiently close such that the first-order perturbative expansion $\omega_\mathrm{g}/\omega_\mathrm{f} \approx 1 + (\gamma/\omega_\mathrm{f})\varepsilon'$ holds with $\varepsilon' << 1$. If*

$$\frac{V_\mathrm{g}^2 \kappa_\mathrm{v}^2 \kappa_\mathrm{i}^2}{(L_\mathrm{f}+L_\mathrm{g})^2 \omega_\mathrm{f}^2} > \sigma^2 \left(\frac{\sqrt{\beta}}{2} + \frac{2}{\sqrt{\beta}} - 2 \right) + \frac{8\gamma^2}{{\omega_\mathrm{f}}^2 \sqrt{\beta}}\,, \quad (28)$$

then the inverter terminal voltage exhibits oscillations at the external forcing frequency, ω_g.

Proof. The condition in (28) follows from substituting $F = V_\mathrm{g}\kappa_\mathrm{v}\kappa_\mathrm{i}/(L_1\omega_\mathrm{f})$ and $k = \gamma/\omega_\mathrm{f}$ in (22). □

C. Numerical Simulation

We compute the feasible region for synchronization of the inverter to the grid by leveraging the condition specified in Lemma 1, for a grid of 200 samples of forcing amplitude, V_g, evenly spaced between $0\,\mathrm{V}$ and $169\,\mathrm{V}$ and a grid of 100 samples of forcing frequency, ω_g, evenly spaced between $59.5\,\mathrm{Hz}$ and $60.5\,\mathrm{Hz}$. The simulation parameters are as follows: $\kappa_\mathrm{v} = 126\,\mathrm{V/V}$, $\kappa_\mathrm{i} = 0.015\,\mathrm{A/V}$, $\alpha = 4.06\,\mathrm{A/V^3}$, $\sigma = 6.09\,\Omega^{-1}$, $L_\mathrm{f} = 1.8\,\mathrm{mH}$, $L_\mathrm{g} = 0.9\,\mathrm{mH}$, $C_\mathrm{f} = 25\,\mu\mathrm{F}$. The region shaded green in Fig. 5 represents the space of forcing amplitudes for which entrainment can be guaranteed.

V. Conclusions and Future Work

In this paper, we provided several compelling extensions to virtual oscillator control. First, we developed a coordinate transformation with which droop-like relationships can be generated to relate the terminal voltage and frequency to real and reactive power output for arbitrary networks. Through time-domain simulations, we demonstrated the superior performance of VOC compared to droop when considering synchronization from cold start, as well as the addition of inverters. Finally, we examined entrainment of a VO-controlled inverter to a stiff voltage source. As part of future work, we will attempt to translate the entrainment conditions into design strategies. Furthermore, we will also explore design strategies for networks that are not purely inductive or resistive. Strategies to regulate active- and reactive-power output in grid-connected mode will also be investigated.

Acknowledgments

M. Sinha and S. V. Dhople were supported in part by the Institute of Renewable Energy and the Environment, UMN, under grant RL-0010-13; the Office of Naval Research under grant N000141410639; and the National Science Foundation under the CAREER award ECCS-1453921. B. B. Johnson and N. G. Ainsworth were supported by the Laboratory Directed Research and Development Program at NREL and by the U.S. Department of Energy under Contract No. DE-AC36-08-GO28308 with NREL. F. Dörfler was supported in part by the Swiss National Science Foundation AP Energy Grant 160573 and by ETH Zürich Startup Funds.

References

[1] M. C. Chandorkar, D. M. Divan, and R. Adapa, "Control of parallel connected inverters in standalone AC supply systems," *IEEE Trans. Ind. Appl.*, vol. 29, no. 1, pp. 136–143, 1993.

[2] J. Vasquez, J. Guerrero, A. Luna, P. Rodriguez, and R. Teodorescu, "Adaptive droop control applied to voltage-source inverters operating in grid-connected and islanded modes," *IEEE Trans. Ind. Electron.*, vol. 56, pp. 4088–4096, Oct. 2009.

[3] Q.-C. Zhong, "Robust droop controller for accurate proportional load sharing among inverters operated in parallel," *IEEE Trans. Ind. Electron.*, vol. 60, no. 4, pp. 1281–1290, 2013.

[4] R. Majumder, A. Ghosh, G. Ledwich, and F. Zare, "Angle droop versus frequency droop in a voltage source converter based autonomous microgrid," in *IEEE PES General Meeting*, pp. 1–8, July 2009.

[5] B. B. Johnson, S. V. Dhople, A. O. Hamadeh, and P. T. Krein, "Synchronization of Parallel Single-Phase Inverters With Virtual Oscillator Control," *IEEE Trans. Power Electron.*, vol. 29, pp. 6124–6138, November 2014.

[6] M. Sinha, F. Dörfler, B. B. Johnson, and S. V. Dhople, "Uncovering Droop Control laws embedded within the nonlinear dynamics of Van der Pol oscillators," *IEEE Trans. Control of Networked Sys.*, 2014. In review.

[7] B. B. Johnson, S. V. Dhople, A. O. Hamadeh, and P. T. Krein, "Synchronization of Nonlinear Oscillators in an LTI Electrical Power Network," *IEEE Trans. Circuits Syst. I, Reg. Papers*, vol. 61, pp. 834–844, March 2014.

[8] B. B. Johnson, M. Sinha, N. Ainsworth, F. Dörfler, and S. V. Dhople, "Synthesizing Virtual Oscillators to control Islanded Inverters," *IEEE Trans. Power Electron.*, 2015. In review.

[9] R. H. Rand, "Lecture notes on nonlinear vibrations," 2012.

[10] S. H. Strogatz, *Nonlinear Dynamics and Chaos: With Applications to Physics, Biology, Chemistry, and Engineering*. Studies in nonlinearity, Westview Press, 1 ed., Jan. 2001.

[11] H. K. Khalil, *Nonlinear Systems*. Prentice Hall, 3 ed., 2002.

[12] S. E. Tuna, "Synchronization analysis of coupled lienard-type oscillators by averaging," *Automatica*, vol. 48, no. 8, pp. 1885–1891, 2012.

[13] F. Wang, J. Duarte, and M. Hendrix, "Active and reactive power control schemes for distributed generation systems under voltage dips," in *IEEE Energy Conversion Congress and Exposition*, pp. 3564–3571, Sept 2009.

[14] F. Z. Peng and J.-S. Lai, "Generalized instantaneous reactive power theory for three-phase power systems," *IEEE Trans. Instrum. Meas.*, vol. 45, Feb 1996.

[15] Q.-C. Zhong and Y. Zeng, "Parallel operation of inverters with different types of output impedance," in *Industrial Electronics Society, IECON 2013-39th Annual Conference of the IEEE*, pp. 1398–1403, IEEE, 2013.

[16] A. Micallef, M. Apap, C. Spiteri-Staines, J. M. Guerrero, and J. C. Vasquez, "Reactive power sharing and voltage harmonic distortion compensation of droop controlled single phase islanded microgrids," *IEEE Transactions on Smart Grid*, vol. 5, pp. 1149–1158, May 2014.

[17] J. Guckenheimer and P. Holmes, *Nonlinear oscillations, dynamical systems, and bifurcations of vector fields*, vol. 42. Springer Science & Business Media, 1983.